Inclusive J/ψ production in forward proton-proton and proton-lead collisions at high energy

Patricia Gimeno-Estivill,[*] Tuomas Lappi,[†] and Heikki Mäntysaari[‡]

Department of Physics, University of Jyväskylä, P.O. Box 35, 40014 University of Jyväskylä, Finland and Helsinki Institute of Physics, P.O. Box 64, 00014 University of Helsinki, Finland

(Received 16 September 2024; accepted 25 October 2024; published 18 November 2024)

We calculate the cross section for forward J/ψ production in proton-proton and minimum bias proton-lead collisions using the color glass condensate (CGC) and nonrelativistic QCD (NRQCD) formalism consistently with deep inelastic scattering data. The cross section for color singlet states is sensitive to a four-point correlator of Wilson lines for which we describe in the Gaussian approximation in the large-N_c limit. Furthermore, we quantify the importance of finite-N_c corrections to have a small ∼12% effect. In contrast with the generic NRQCD expectation, we show that the color singlet contribution is only 15% to the total cross section. We also compare our predictions for J/ψ production as well as for the nuclear modification ratio R_{pPb} to LHCb and ALICE data. We find a good agreement at forward rapidities, except at low transverse momenta where the cross sections are overestimated.

DOI: 10.1103/PhysRevD.110.094035

I. INTRODUCTION

Abundant data on J/ψ production in proton-proton and proton-nucleus collisions at high energy is available from different measurements performed at RHIC [1–3] and at the LHC [4–9]. These processes are especially powerful in probing QCD dynamics in the region where gluon saturation effects are expected to be important. This is because the J/ψ mass is optimally suitable for such studies: It is heavy enough to ensure the validity of perturbative calculations but low enough for saturation effects to be clearly visible. Furthermore, because of the heavy quark mass, it should also be possible to understand the quark-antiquark hadronization process in a weak coupling framework.

In this paper, we consider J/ψ production at forward rapidities, where a proton-nucleus collision can be described in the color glass condensate (CGC) effective field theory as an interaction between a "dilute" proton probe and a "dense" system of gluons in the target nucleus [10–13]. This picture is valid at high energy (small momentum fraction x), where gluon saturation is predicted by the CGC. In this framework, the lowest-order (LO) process in the strong coupling constant α_s is a projectile gluon splitting into a charm quark pair either before or after interacting with the target. The production amplitude for a heavy quark pair at LO in α_s was computed in Ref. [14] in the dilute-dense approximation.

Historically [15,16] it was argued that the dominant contribution to J/ψ production at small momentum transfer $p_\perp$ comes from the fusion of two gluons in a color singlet channel. This color singlet model (CSM) is still widely used in the literature; see, e.g., Ref. [17] for a review. In more recent studies [18–21], the color octet contributions were also included in the color evaporation model (CEM), which results in a good agreement with RHIC and LHC data.

Nevertheless, the overall normalization in the CEM model is typically adjusted by hand to measured cross section data, limiting the universality and predictive power of the approach. This calls for a more systematical framework, which can be provided by the nonrelativistic QCD (NRQCD) formalism [22]. Here, the starting point is the observation that the heavy mass of the quarks makes the quarkonium system approximatively nonrelativistic. As a consequence, its hadronization into a physical J/ψ particle can then be factorized and described in terms of long-distance matrix elements (LDMEs) [23]. These are universal nonperturbative quantities that can be extracted from experimental data [24].

Our goal is to test the predicted contribution of the different intermediate quantum states κ to the J/ψ production cross section in forward proton-proton ($p+p$) and minimum bias proton-lead ($p+\mathrm{pb}$) collisions in the CGC + NRQCD framework. In this NRQCD factorization formalism, the J/ψ production cross section for different

[*]Contact author: patricia.p.gimenoestivill@jyu.fi
[†]Contact author: tuomas.v.v.lappi@jyu.fi
[‡]Contact author: heikki.mantysaari@jyu.fi

$c\bar{c}$ quantum states was first calculated in Ref. [25], and phenomenological applications were reported in Refs. [26,27]. In the latter, an approximated form of the four-point quadrupole correlator of Wilson lines describing the interaction of the probe was considered. In contrast to these works, we use the quadrupole derived in Ref. [28] in the large-N_c limit in the Gaussian approximation, and we also quantify the importance of the finite-N_c corrections. Unlike earlier phenomenological studies using CGC + NRQCD, the quadrupole and dipole correlators present in the cross section are evolved with the Balitsky-Kovchegov (BK) equation [29,30] from an initial condition with all the parameters obtained consistently from deep inelastic scattering (DIS) data. We also use a realistic description of the nuclear geometry with an impact parameter ($\boldsymbol{b}_\perp$)-dependent saturation scale following Ref. [31], an approach that has been successfully used in Refs. [21,32–34]. Our results for the differential cross section in proton-proton ($p+p$) and proton-lead ($p+\mathrm{pb}$) collisions as well as the nuclear modification factor are compared to the LHCb [4,5] and ALICE data [9].

We begin this paper with a description of the CGC + NRQCD framework in Sec. II. The phenomeonological study is presented in Sec. III, where we first quantify the importance of finite-N_c corrections to the quadrupole correlator, and then compare our predictions for the J/ψ spectra and the nuclear modification factor to the LHCb and ALICE data. We conclude with a summary in Sec. IV.

II. CGC + NRQCD FACTORIZATION FORMALISM

The cross section for J/ψ production with transverse momentum $\boldsymbol{p}_\perp$ and rapidity y is expressed in NRQCD factorization as [25]

$$\frac{\mathrm{d}\sigma^{\mathrm{J}/\psi}}{\mathrm{d}^2\boldsymbol{p}_\perp dy} = \sum_\kappa \frac{\mathrm{d}\hat{\sigma}^\kappa}{\mathrm{d}^2\boldsymbol{p}_\perp \mathrm{d}y} \langle \mathcal{O}_\kappa^{J/\psi} \rangle. \tag{1}$$

Here, the short distance partonic cross sections $\mathrm{d}\hat{\sigma}^\kappa$ can be calculated perturbatively in the CGC framework and represent the production of an intermediate heavy quark pair in a state κ. The sum in Eq. (1) includes all the possible quantum configurations $\kappa = {}^{2s+1}L_J^{[c]}$, where S, L, and J are, respectively, the spin, orbital angular momentum, and total angular momentum. The superscript c denotes the color state of the intermediate quark pair, which can be in a color singlet ($c=1$) or octet ($c=8$) configuration. On the other hand, the low-energy hadronization of these intermediate heavy quark states into a physical bound state is represented by the long-distance matrix elements (LDMEs) $\langle \mathcal{O}_\kappa^{\mathrm{J}/\psi} \rangle$. They are universal and nonperturbative, determined by fitting experimental data [24].

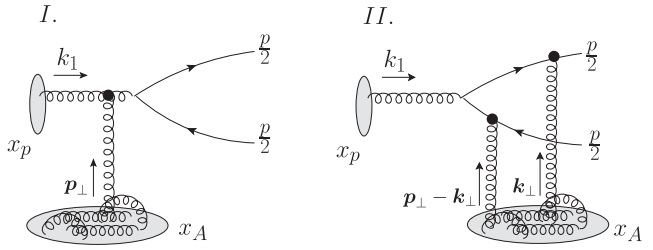

FIG. 1. Proton-nucleus collision where a gluon with momentum k_1 from the projectile proton splits into an on-shell quark and antiquark with momentum $p/2$ either after (diagram I) or before (diagram II) interacting with the gluon field in the target nucleus. The black dots denote the Wilson Lines that resum the multiple interactions of the partons when crossing the shockwave. The complete calculation of the amplitude for this process can be found in Ref. [14].

A. Quarkonium production: short-distance partonic cross sections

The short-distance creation of a heavy quark pair in forward proton-nucleus collisions is depicted in Fig. 1. There, the symbol $x_p(x_A)$ is the fraction of the proton (nucleus) longitudinal momentum carried by the produced particle,

$$x_{p,A} = \frac{\sqrt{m_{\mathrm{J}/\psi}^2 + \boldsymbol{p}_\perp^2}}{\sqrt{s}} e^{\pm y}, \tag{2}$$

where $\sqrt{s}$ is the center-of-mass energy, $y = \ln(p^+/p^-)/2$ the rapidity, and $\boldsymbol{p}_\perp$ the transverse momentum of the produced J/ψ particle with mass $m_{\mathrm{J}/\psi} = 3.097$ GeV ($\approx 2m_c$). We use the light-cone notation $x^\pm = (x^0 \pm x^3)/\sqrt{2}$ for coordinates and $p^+ \approx \sqrt{2}E \gg p^- = (m_{\mathrm{J}/\psi}^2 + \boldsymbol{p}_\perp^2)/2p^+$ for momenta. The large rapidity y in the forward region implies that $x_A \ll 1$ and $x_p \sim 1$ so that the collision can be described as a dilute probe interacting with the small-x gluon field of the target nucleus in the CGC formalism. Further, we consider the proton in the collinear limit where the incoming parton has no transverse momentum ($k_{1\perp} \to 0$). This is because the transverse momentum of the gluons in the proton is much smaller than the mass and transverse momentum of the produced J/ψ particle: $k_{1\perp} \sim \Lambda_{\mathrm{QCD}} \ll m_{\mathrm{J}/\psi}$ and $k_{1\perp} \sim \Lambda_{\mathrm{QCD}} \ll p_\perp$. This collinear gluon can split into a quark-antiquark pair before or after the collision where transverse momentum from the small-x_A gluons in the nucleus is transferred to the partons (gluon or quark pair).

In this framework, the short-distance partonic cross sections for the heavy quark pair production in color octet (CO) or color singlet (CS) states, respectively, read [25]

$$\frac{\mathrm{d}\hat{\sigma}}{\mathrm{d}^2\boldsymbol{p}_\perp \mathrm{d}y} \overset{\mathrm{CO}}{=} \int_{\boldsymbol{b}_\perp} \frac{\alpha_\mathrm{s}}{4(2\pi)^3(N_c^2-1)} x_p f_{p/g}(x_p,\mu^2) \times \int_{\boldsymbol{k}_\perp} \mathcal{N}(\boldsymbol{k}_\perp)\mathcal{N}(\boldsymbol{p}_\perp-\boldsymbol{k}_\perp)\tilde{\Gamma}_8^\kappa(p_\perp,k_\perp), \quad (3)$$

and

$$\frac{\mathrm{d}\hat{\sigma}}{\mathrm{d}^2\boldsymbol{p}_\perp \mathrm{d}y} \overset{\mathrm{CS}}{=} \int_{\boldsymbol{b}_\perp} \frac{\alpha_\mathrm{s}}{4(2\pi)^3(N_c^2-1)} x_p f_{p/g}(x_p,\mu^2) \times \int_{\boldsymbol{\Delta}_\perp,\boldsymbol{r}_\perp,\boldsymbol{r}'_\perp} e^{-i\boldsymbol{p}_\perp\boldsymbol{\Delta}_\perp}(Q - D_{\boldsymbol{r}_\perp}D_{\boldsymbol{r}'_\perp})\tilde{\Gamma}_1^\kappa(r_\perp,r'_\perp), \quad (4)$$

where $Q \coloneqq Q_{\frac{\boldsymbol{r}_\perp}{2},\boldsymbol{\Delta}_\perp+\frac{\boldsymbol{r}'_\perp}{2},\boldsymbol{\Delta}_\perp-\frac{\boldsymbol{r}'_\perp}{2},-\frac{\boldsymbol{r}_\perp}{2}}$ is the quadrupole, and we use the short-hand notation $\int_\perp = \int \mathrm{d}^2_\perp$. For proton-proton collisions, we assume that the impact parameter dependence factorizes and the integral over the impact parameter $\boldsymbol{b}_\perp$ results in the transverse area of the proton. We use the value $\pi R_p^2 = 16.36$ mb, which is determined in the fit to DIS structure function data [31] that we use in this work. On the other hand, when we consider minimum bias proton-nucleus collisions, we account for the impact-parameter profile of the nucleus explicitly. Here, $x_p f_{p,g}(x_p,\mu^2)$ is the proton collinear gluon distribution function, for which we use the MSHT20 LO pdf [35] with $\mu^2 = m_{\mathrm{J}/\psi}^2$. The sensitivity of our results on the scale choice is quantified in Sec. III. The strong coupling is set to $\alpha_\mathrm{s} = 0.24$ [22], and it is a source of uncertainty in the normalization of the cross section.

The hard matrix elements $\tilde{\Gamma}_8^\kappa(p_\perp,k_\perp)$ and $\tilde{\Gamma}_1^\kappa(r_\perp,r'_\perp)$ are given in Appendices B. 1 and B. 2 in Ref. [25]. Moreover, $\boldsymbol{r}_\perp = \boldsymbol{x}_\perp - \boldsymbol{y}_\perp$ is the transverse size of the dipole shown in Fig. 1, and $\boldsymbol{r}'_\perp$ is the corresponding size in the complex conjugate amplitude. The coordinate $\boldsymbol{\Delta}_\perp = (\boldsymbol{x}'_\perp + \boldsymbol{y}'_\perp - \boldsymbol{x}_\perp - \boldsymbol{y}_\perp)/2$ represents the distance between the centers of the dipoles in the amplitude and in the complex conjugate amplitude.

The functions $\mathcal{N}(\boldsymbol{k}_\perp)$ and $\mathcal{N}(\boldsymbol{p}_\perp-\boldsymbol{k}_\perp)$ in the cross section for color octet states in Eq. (3) are the Fourier transformed two-point correlators (dipoles) in momentum space,

$$\mathcal{N}(\boldsymbol{k}_\perp) = \int_{\boldsymbol{r}_\perp} e^{i\boldsymbol{k}_\perp\boldsymbol{r}_\perp} D_{\boldsymbol{r}_\perp}, \quad (5)$$

where

$$D_{\boldsymbol{r}_\perp} = \frac{1}{N_\mathrm{c}}\langle \mathrm{Tr}[V_F(0)V_F^\dagger(\boldsymbol{r}_\perp)]\rangle_{y_A}. \quad (6)$$

This dipole is the eikonal (high-energy) scattering amplitude of a quark-antiquark pair off a dense target gluon field, where $\langle\ldots\rangle_{y_A}$ represents the average over the color charge densities of the target nucleus evaluated at the evolution rapidity $y_A = \ln\frac{x_0}{x}$ [10]. The Wilson Lines $V_{F,A}(\boldsymbol{x}_\perp)$ are defined as

$$V_{F,A}(\boldsymbol{x}_\perp) = \mathcal{P}\exp\left(-ig\int \mathrm{d}x^+ A_a^-(x^+,\boldsymbol{x}_\perp)t^a\right), \quad (7)$$

where $\mathcal{P}$ is a path ordering operator and A^- the classical gluon field in the target nucleus. The SU(3) color matrices t^a are in the fundamental (F) or adjoint (A) representation for quark and gluon probes, respectively.

The energy (Bjorken-x) dependence of the dipole correlator in Eq. (6) can be obtained by solving the running coupling Balitsky-Kovchegov (rcBK) equation [29,30,36] in the large-N_c limit. In Ref. [31], the initial condition for this evolution at $x_0 = 0.01$ was considered to take a form inspired by the McLerran-Venugopalan (MV) model as [37]

$$\mathcal{N}(\boldsymbol{r}_\perp) = 1 - \exp\left[-\frac{(\boldsymbol{r}_\perp^2 Q_{s0}^2)^\gamma}{4}\ln\left(\frac{1}{|\boldsymbol{r}_\perp|\Lambda_\mathrm{QCD}} + e_c\cdot e\right)\right], \quad (8)$$

where $\Lambda_\mathrm{QCD} = 0.241$ GeV. We use here the MV^e fit of Ref. [31], where γ is fixed to $\gamma = 1$, and the free parameters $Q_{s0}^2 = 0.060$ GeV^2 and $e_c = 18.9$ are determined by a fit to the HERA inclusive DIS cross section data [38]. For a nuclear target, the rcBK evolution equation is solved separately for each impact parameter $\boldsymbol{b}_\perp$ using an initial condition where the $\boldsymbol{b}_\perp$ dependence of the saturation scale is obtained from the optical Glauber model:

$$\mathcal{N}^A(\boldsymbol{r}_\perp,\boldsymbol{b}_\perp) = 1 - \exp\left[-AT_A(\boldsymbol{b}_\perp)\pi R_p^2\frac{(\boldsymbol{r}_\perp^2 Q_{s0}^2)^\gamma}{4}\right] \times \ln\left(\frac{1}{|\boldsymbol{r}_\perp|\Lambda_\mathrm{QCD}} + e_c\cdot e\right). \quad (9)$$

Here, $T_A(\boldsymbol{b}_\perp)$ is the Woods-Saxon nuclear density normalized to unity: $\int \mathrm{d}^2\boldsymbol{b}_\perp T_A(\boldsymbol{b}_\perp) = 1$. In the region where the nuclear saturation scale would fall below that of the proton, we replace the dipole-nucleus scattering amplitude by the dipole-proton amplitude scaled such that all nontrivial nuclear effects vanish. Further details can be found in Ref. [31]. We emphasize that in Eq. (9), there are no additional free parameters for the nucleus apart from the standard Woods-Saxon density. Thus, the nuclear modification of cross sections is a pure prediction of the framework without any additional fit parameters.

In Eq. (4), the cross section for color singlet states is sensitive to dipoles (D) and a quadrupole (Q). The quadrupole is defined as

$$Q = \frac{1}{N_c}\left\langle \mathrm{Tr}[V_F(\boldsymbol{x}_\perp)V_F^\dagger(\boldsymbol{x}'_\perp)V_F(\boldsymbol{y}_\perp)V_F^\dagger(\boldsymbol{y}'_\perp)]\right\rangle_{y_A}, \quad (10)$$

where $Q \coloneqq Q_{\boldsymbol{x}_\perp \boldsymbol{x}'_\perp \boldsymbol{y}_\perp \boldsymbol{y}'_\perp}$. This expression is not reducible to a product of dipoles neither for a large nucleus nor in the large-N_c limit [39]. However, in the Gaussian approximation [40,41], the color charge correlators are assumed to be Gaussian even after evolution, and the quadrupole can be rewritten in terms of two-point correlation functions. Unlike previous studies of inclusive heavy quarkonium production, we use the explicit Gaussian approximation for the quadrupole in the large-N_c limit as well as at finite N_c. The explicit expressions are given, respectively, by Eqs. (B.22) and (B.21) in Ref. [28]. The accuracy of the Gaussian approximation at the initial condition of the small-x JIMWLK evolution [42] and after a relatively long evolution has been shown in Ref. [43]. The importance of an accurate description of the quadrupole in the case of inclusive dihadron production has been demonstrated in Ref. [44].

B. Hadronization: long-distance matrix elements

In the NRQCD formalism, the J/ψ state can be written as a power series in the relative velocity $v \ll 1$ of the heavy quark pair [45],

$$\begin{aligned}|J/\psi\rangle = {} & O(1)|^3S_1^{[1]}\rangle + O(v)|^3P_J^{[8]}g\rangle + O(v^2)|^1S_0^{[8]}g\rangle \\ & + O(v^2)|^3S_1^{[8]}gg\rangle + \ldots, \end{aligned} \quad (11)$$

where the dominant Fock state involves the quark-antiquark pair in a color singlet state and quantum numbers that are consistent with the physical vector meson[1] with $J^{PC} = 1^{--}$. The quantum numbers of higher Fock states are selected according to conservation of total angular momentum J, parity P, and charge conjugation C in the heavy quark Lagrangian, and their contribution in the velocity expansion in Eq. (11) is determined by the energy shift with respect to the dominant state [23]. The soft gluons present in higher Fock states can be emitted before the bound state is formed and thus changing the color and spin of the intermediate heavy quark pair. This effect is included in universal long-distance matrix elements (LDMEs), which can be written as vacuum expectation values of four-fermion operators with the NRQCD heavy quark Lagrangian [22]. Their hierarchy in powers of velocity is established according to NRQCD power counting rules [22], and their specific values are determined by fitting decay width or cross sections data. The four independent LDMEs used in the phenomenology study of J/ψ production in Sec. III are listed in Table I.

[1]Quarkonium $^{2S+1}L_J^{[c]}$ states have parity $P = (-1)^{L+1}$ and charge conjugation $C = (-1)^{L+S}$.

TABLE I. Values of LDMEs used in this work and their corresponding order in velocity. The LDME for the color singlet state $^3S_1^{[1]}$ is estimated using the value of the J/ψ wave function at the origin in the Buchmüller and Tye potential model in Ref. [46]. The LDMEs for the color octet states $^1S_0^{[8]}$,$^3P_0^{[8]}$, and $^3S_1^{[8]}$ are determined by fitting NLO collinearly factorized pQCD + NRQCD results to Tevatron prompt J/ψ yields in Ref. [47]. The statistical uncertainties correspond to the mass dependence of the LDMEs.

$\langle\mathcal{O}(^3S_1^{[1]})\rangle\ O(v^0)$	$1.16/(2N_c)$ GeV^3
$\langle\mathcal{O}(^1S_0^{[8]})\rangle\ O(v^3)$	0.089 ± 0.0098 GeV^3
$\frac{\langle\mathcal{O}(^3P_0^{[8]})\rangle}{m_c^2}\ O(v^4)$	0.0056 ± 0.0021 GeV^3
$\langle\mathcal{O}(^3S_1^{[8]})\rangle\ O(v^4)$	0.0030 ± 0.0012 GeV^3

The P-wave LDMEs with $J = 1, 2$ that contribute at the same order in velocity as the operator $\langle\mathcal{O}(^3P_0^{[8]})\rangle$ can be obtained using heavy quark spin symmetry [22]:

$$\langle\mathcal{O}(^3P_J^{[8]})\rangle = (2J+1)\langle\mathcal{O}(^3P_0^{[8]})\rangle[1 + \mathcal{O}(v^2)]. \quad (12)$$

Accordingly, the contribution of the P-wave states in the cross section is

$$\begin{aligned}\sum_{J=0}^{2}\langle^3P_J^{[8]}\rangle \mathrm{d}\hat{\sigma}^{^3P_J^{[8]}} &= \langle^3P_0^{[8]}\rangle \mathrm{d}\hat{\sigma}^{^3P_0^{[8]}} + 3\langle^3P_0^{[8]}\rangle \mathrm{d}\hat{\sigma}^{^3P_1^{[8]}} \\ &\quad + 5\langle^3P_0^{[8]}\rangle \mathrm{d}\hat{\sigma}^{^3P_2^{[8]}} \\ &= 9\langle^3P_0^{[8]}\rangle \mathrm{d}\hat{\sigma}^{^3P_{\mathrm{avg}}^{[8]}}, \end{aligned} \quad (13)$$

where we have defined the following weighted average P-wave short-distance coefficient:

$$\mathrm{d}\hat{\sigma}^{^3P_{\mathrm{avg}}^{[8]}} = \frac{1}{9}\left(\mathrm{d}\hat{\sigma}^{^3P_0^{[8]}} + 3\mathrm{d}\hat{\sigma}^{^3P_1^{[8]}} + 5\mathrm{d}\hat{\sigma}^{^3P_2^{[8]}}\right). \quad (14)$$

Although the color singlet LDME is dominant in powers of velocity, when the hard matrix elements $\tilde{\Gamma}_8^\kappa(p_\perp, k_\perp)$ and $\tilde{\Gamma}_1^\kappa(r_\perp, r'_\perp)$ in Eqs. (3) and (4) are expanded[2] in powers of $m_{J/\psi}/p_\perp$, the color octet channels become important at large transverse momentum $p_\perp \sim Q_s \gg m_{J/\psi}$. In this region, by normalizing the $^3S_1^{[8]}$ channel as $\mathcal{O}(1)$, the other color octet channels behave as $\mathcal{O}(m_{J/\psi}^2/p_\perp^2)$, and the color singlet $^3S_1^{[1]}$ contribution is suppressed by $\mathcal{O}(m_{J/\psi}^4/p_\perp^4)$ [25]. Therefore, the expectation from a pure power counting argument would be to have the color singlet state dominant

[2]The correlators are assumed to not contribute any power behavior. We refer the reader to Ref. [25] for details of the calculation.

at small $p_\perp \ll M$, accompanied by a higher contribution from color octet channels at high $p_\perp$.[3]

III. RESULTS

Given the dipole-proton scattering amplitude obtained from DIS fits [31] and the values of the LDMEs in Table I, we can next calculate cross sections for inclusive forward J/ψ production in proton-proton ($p+p$) and proton-lead ($p+\mathrm{pb}$) collisions. We emphasize that our results are genuine predictions with no free parameters: The dipole amplitude has been fit to DIS data, the extension to nuclei only requires a standard Wood-Saxon density, and the LDMEs have been extracted in a different kinematical regime completely independently from our analysis.

A. Finite-N_c corrections

The quadrupole operator in Eq. (10) cannot be factorized in terms of dipoles. Instead, as already discussed in Sec. II A, we evaluate it in the Gaussian approximation for which the finite-N_c corrections can be included following Ref. [28]. As an input, the Gaussian approximation requires a dipole amplitude $D_{\boldsymbol{r}_\perp}$ obtained by solving the BK equation in the large-N_c limit.

Although parametrically one expects ∼10% finite-N_c corrections to the BK evolution, such corrections in practice turn out to be much smaller, of the order 0.1% at leading order [48] (and somewhat larger at next-to-leading order [49]). Hence, when we determine the importance of the finite-N_c corrections for J/ψ production, it is enough to include finite-N_c terms in the quadrupole operator.

Using the Gaussian approximation, we show in Fig. 2 the $p_\perp$ spectra for the inclusive J/ψ production cross section in $p+p$ collisions in the color singlet channel, where the J/ψ is in the ${}^3S_1^{[1]}$ state.[4] The finite-N_c correction is found to be small, of the order of $1/N_c^2 \sim 12\%$ at all $p_\perp$. Thus, we consider the large-N_c limit to be a suitable approximation in the leading order calculation presented in this work, although finite-N_c corrections might be required for precision level data comparisons.

Additionally, we show in Fig. 2 the cross section obtained by using an approximative form of the quadrupole, written in Eq. (5) of Ref. [26] and used in previous phenomenological studies [27,50,51]. The approximative quadrupole is found to underestimate the cross section at low $p_\perp$ and overestimate it at high-$p_\perp$, maximally by a factor ∼2. Based on this result, we conclude that a more accurate description of the quadrupole operator, e.g., in the Gaussian approximation employed here, is necessary in order to accurately predict the cross section in the color singlet channel.

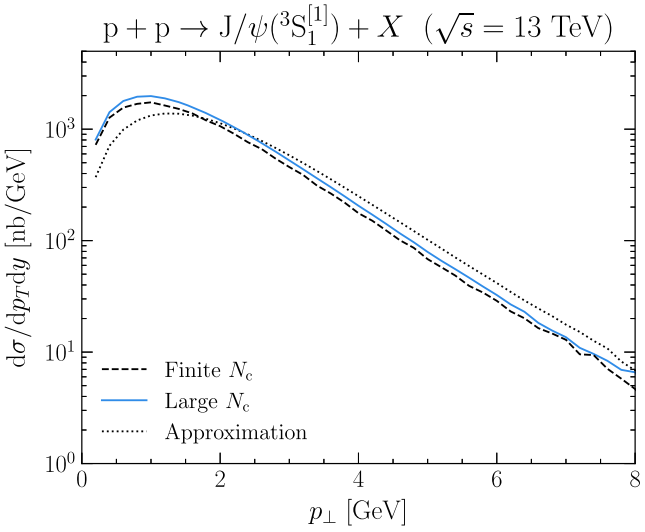

FIG. 2. Differential J/ψ production cross section through the color singlet channel ${}^3S_1^{[1]}$ in proton-proton collisions at center-of-mass energy $\sqrt{s} = 13$ GeV and rapidity $y = 3.25$. The dashed line is calculated with the complete expression of the quadrupole at finite-N_c, the solid line corresponds to the calculation with the quadrupole in the large-N_c limit, and the dotted line is computed with the quadrupole approximation taken from Ref. [26].

B. CGC + NRQCD in small collision systems

In Figs. 3 and 4, we show the transverse momentum distribution of the produced J/ψ in $p+p$ and $p+\mathrm{pb}$ collisions, respectively. The results are compared with the LHCb [4,5] and ALICE [9] data. The ALICE data corresponds to inclusive J/ψ production and thus also includes a nonprompt contribution not included in our calculation. As it is illustrated in both figures, the differential cross section as a sum of the individual channels overestimates the experimental data by a factor ∼5…10 at small $p_\perp$. Nevertheless, it is remarkable that a good agreement of the data is found at moderately large $p_\perp \gtrsim 5$ GeV using the LDME extracted from a fit using NLO collinear factorization [47]. Therefore, the LO calculation in the CGC presented in this work captures some features of the collinear NLO calculations, which are already consistent with experimental data at large $p_\perp$ [27,52,53].

Looking at the individual contributions in Figs. 3 and 4, the dominant channel throughout the $p_\perp$ spectra is the color octet ${}^1S_0^{[8]}$ channel. This has a contribution of about 70% on the total $p_\perp$ integrated cross section in both $p+p$ and $p+\mathrm{pb}$ collisions. Although NRQCD predicts the color

[3]In the proton collinear approximation, all the quarkonium transverse momentum is given by the nuclear target at small x, with parametrically $k_\perp \sim Q_s$. Hence, the kinematic region $p_\perp \gg Q_s$ would also get a larger contribution from next-to-leading order (NLO) processes in α_s where a recoiling particle can balance the quarkonium momentum $p_\perp$ in the final state.

[4]Note that the color octet channel does not depend on the quadrupole and does not have a similar finite-N_c correction.

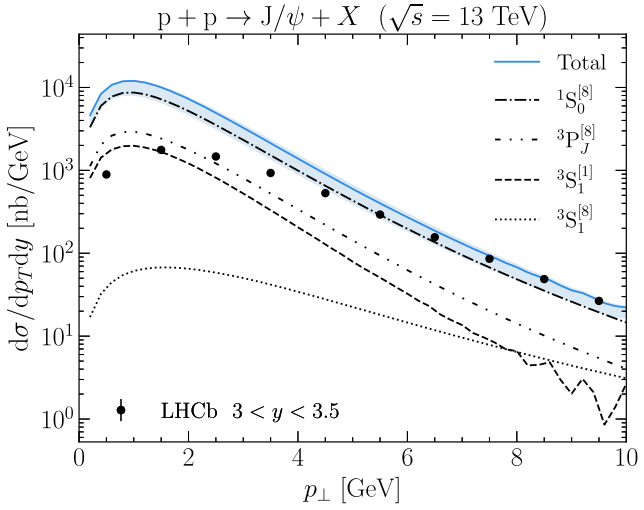

FIG. 3. Differential J/ψ production cross section in proton-proton collisions as a function of $p_\perp$, rapidity $y = 3.25$ and center-of-mass energy $\sqrt{s} = 13$ TeV. The sum of the different channels is represented by the top solid line in blue, which is followed by $^1S_0^{[8]}$, $^3P_J^{[8]}$,$^3S_1^{[1]}$, and $^3S_1^{[8]}$ channels, from top to bottom. The factorization scale is fixed to $\mu^2 = m^2_{J/\psi}$, and the blue uncertainty band includes the variation from $\mu^2 = m_c^2$ to $\mu^2 = m^2_{J/\psi} + p_\perp^2$. The experimental LHCb data for prompt J/ψ production is taken from Ref. [4].

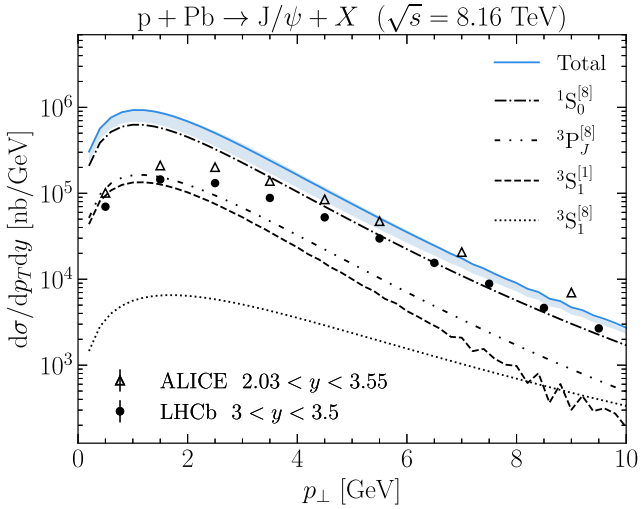

FIG. 4. Differential J/ψ production cross section in proton-lead collisions as a function of $p_\perp$, fixed rapidity $y = 3.25$ and energy $\sqrt{s} = 8.16$ TeV. The sum of the different channels is represented by the top solid line in blue, which is followed by $^1S_0^{[8]}$, $^3P_J^{[8]}$,$^3S_1^{[1]}$, and $^3S_1^{[8]}$ channels, from top to bottom. The factorization scale is fixed to $\mu^2 = m^2_{J/\psi}$, and the blue uncertainty band includes the variation from $\mu^2 = m_c^2$ to $\mu^2 = m^2_{J/\psi} + p_\perp^2$. The LHCb data for prompt J/ψ production is taken from Ref. [5] and the ALICE data for inclusive J/ψ production from Ref. [9].

singlet LDME as the largest in powers of velocity, the relative contribution of the $^3S_1^{[1]}$ channel is approximately 15% of the total in both collisions. By itself, the color singlet channel is close to the experimental data at low $p_\perp$ but always below the color octet contribution. It also falls faster than the color octet channels at high $p_\perp$, in accordance with the expected momentum dependence discussed in the previous Sec. II B.

The small contribution of the color singlet channel could be interpreted as a N_c suppression, since there is one color singlet and $N_c^2 - 1$ color octet configurations. This suppression could also be explained in terms of collinearly factorized pQCD, where at leading twist, the $^3S_1^{[1]}$ singlet state is produced only at $\mathcal{O}(\alpha_s^3)$ [54]. The contribution in the LO CGC formalism here corresponds to a higher twist contribution in collinear factorization at LO [17] and is thus suppressed at large $p_\perp$. This comparison between the two theories could explain the smallness of the singlet contribution, and we expect it to become a larger fraction of the total cross section at high $p_\perp$ at NLO.

We attribute the behavior of the $p_\perp$ spectra to the fixed leading order calculation in α_s and expect that the implementation of the Sudakov term in the cross section is needed to correct the peak position at small $p_\perp$ [55]. This factor should be different for the color singlet and octet channels and thus also affect their relative contributions at a specific $p_\perp$. In particular, the color octet should have a larger Sudakov factor than the singlet, which would increase the mean $p_\perp$ in the octet channels more. Thus, we expect that the inclusion of Sudakov effects would lead to a larger suppression of the color octet channels at small $p_\perp$ than the singlet. A refinement of the cross section including this soft gluon radiation could be done in a future work, e.g., among the lines proposed in Ref. [56].

In order to determine the sensitivity on the factorization scale μ^2, we also show in Figs. 3 and 4 the dependence of the total cross section on the scale choice μ^2. The central values are obtained using our default scale choice $\mu^2 = m^2_{J/\psi}$, and we vary the scale from $\mu^2 = m_c^2$ to $\mu^2 = m^2_{J/\psi} + p_T^2$. The dependence on the scale is modest, affecting the overall normalization up to ∼28%, and in particular, it cannot explain the fact that the presented calculation overestimates the ALICE and LHCb at low p_T.

Inclusive J/ψ production in the color evaporation model (CEM) considers a similar description for the target, but the hadronization is described with a common transition probability, leading to a dominance of color octet channels. The $p_\perp$ spectra obtained in Refs. [21,33] are very similar to our current calculation, which uses the same dipole amplitude and similarly steeper than in the LHCb data. On the other hand, the CGC + NRQCD formalism has been used to successfully reproduce the $p + p$ and $p +$ pb data

in Refs. [26,27], although the contribution of different production channels to the total cross section was not shown in the figures. However, our setup includes various improvements that explain the different cross sections obtained. First, in Refs. [26,27], the approximative form of the quadrupole illustrated in Fig. 2 was used, along with an impact parameter-independent description of the nucleus and a different choice for the factorization scale μ^2. Furthermore, the proton transverse area πR_p^2, which controls the overall normalization, was not taken from the applied DIS fit. Also, an additional 30% systematic uncertainty from higher order α_s corrections was added on top of the statistical uncertainties from the LDMEs. This led to a rather wide error band on the results.

We also note that the LDMEs are not known very precisely; for example, there are sets of LDMEs extracted at next-to-leading order (NLO) with negative values [57–59], and therefore, they could lead to negative cross sections. Furthermore, the initial condition for the small-x BK evolution determined from HERA data including only light quarks has its own uncertainties that could affect the cross section, especially at high p_T [60]. Leading order fits have not been able to simultaneously describe the total cross section and the charm production data, and only light quarks are included in the fit of Ref. [31] that we use here. Consequently, the heavy quark contribution is encoded in the nonperturbative fit parameters, and when the fit is used to calculate charm production, one typically expects to overestimate the cross section, which is also the case here.

A simultaneous description of the total cross section and heavy quark production HERA data is only obtained at NLO accuracy [61]. One could speculate that, similarly, an NLO calculation is needed to correctly describe the normalization of inclusive J/ψ cross sections in hadronic collisions. In particular, the Sudakov effect originated from soft gluon radiation [62] would be needed to improve our calculation. Here, our focus has been to present a self-consistent LO calculation without any free parameters, which we believe is the correct starting point for including higher order effects in a systematic way in the future.

C. Nuclear modification factor and Cronin effect

As discussed in the previous section, there are several uncertainties in the overall normalization of the cross section. However, many of these cancel in the cross section ratio. Thus, we calculate the nuclear modification factor R_{pPb}, for which our approach provides a robust parameter-free prediction. For minimum bias collisions, R_{pPb} is defined as

$$R_{pPb} = \frac{\frac{\mathrm{d}\sigma_{pPb}}{\mathrm{d}^2\boldsymbol{p}_\perp \mathrm{d}y}}{A \times \frac{\mathrm{d}\sigma_{pp}}{\mathrm{d}^2\boldsymbol{p}_\perp \mathrm{d}y}}. \tag{15}$$

Here, $A = 208$ for the lead nucleus. In Fig. 5, we show R_{pPb} for each independent channel at different rapidities.

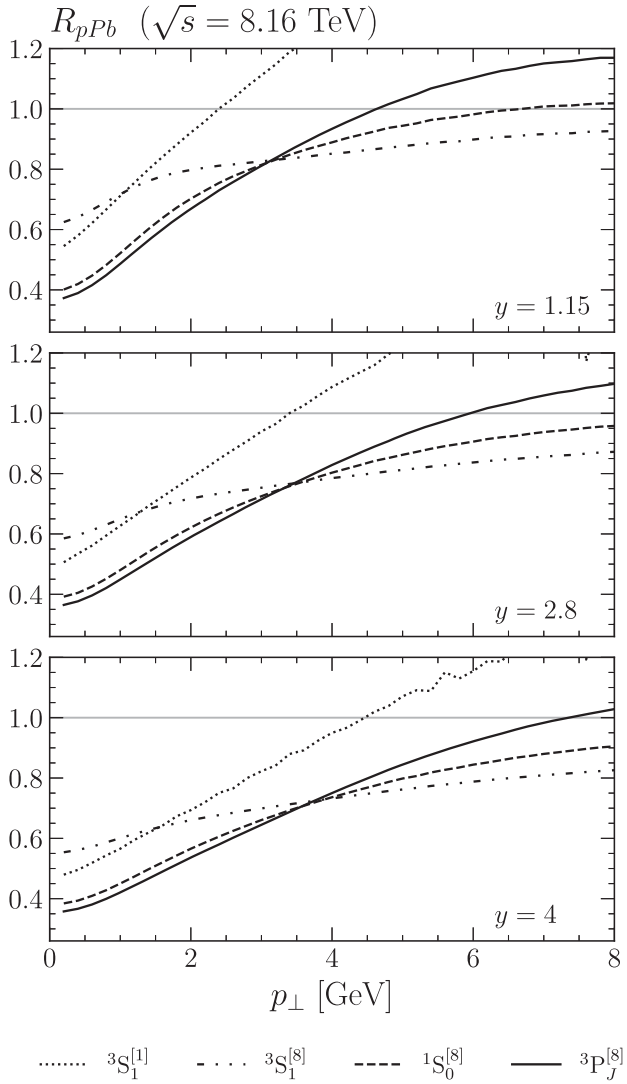

FIG. 5. Nuclear suppression factor R_{pPb} for each independent channel as a function of $p_\perp$ and fixed rapidity. The Cronin effect is reduced as the rapidity increases from $y = 1.5$ to $y = 4$.

We predict a strong nuclear suppression, $R_{pPb} \sim 0.4$, at low J/ψ transverse momentum, resulting from saturation effects. In agreement with the results presented in Ref. [27], there is a strong Cronin enhancement in the color singlet $^3S_1^{[1]}$ channel at intermediate p_T. This phenomenon could be explained in collinear factorization pQCD, where two gluons from the target in the higher-twist diagram are needed to produce a $^3S_1^{[1]}$ state at LO in α_s. Thus, even in the dilute limit at high $p_\perp$, the singlet cross section does not scale as Q_s^2, and consequently $R_{pPb} > 1$. In contrast, for color octet states, the ratio R_{pPb} approaches unity at large $p_\perp$ by construction [31,63].

The nuclear modification factor for J/ψ production as a function of transverse momentum including all production channels is shown in Fig. 6. The level of R_{pPb} reproduces well the rapidity integrated data in the $1.5 < y < 4$ range,

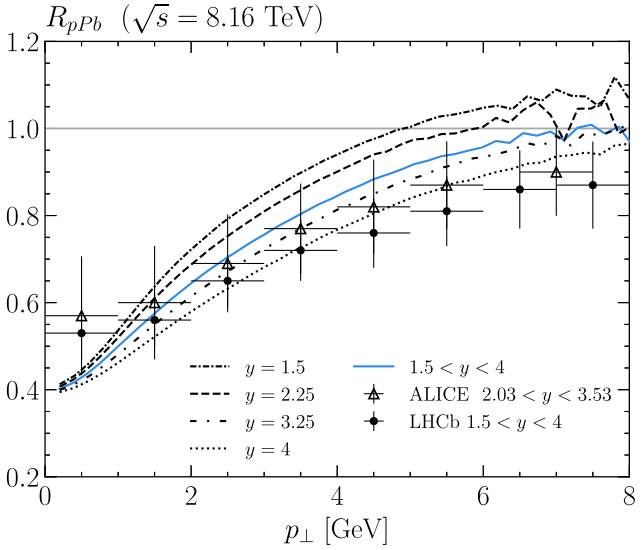

FIG. 6. Nuclear supression factor R_{pPb} as a function of $p_\perp$ at $\sqrt{s} = 8.16$ TeV for individual rapidities $y = 1.5$, 2.25, 3.25, and 4 as well as for the integrated value over $1.5 < y < 4$. The LHCb data [5] for prompt J/ψ production and ALICE data [9] for inclusive J/ψ production include statistical and systematic uncertainties as quadratic sums in the vertical lines. The horizontal error bars are bin widths.

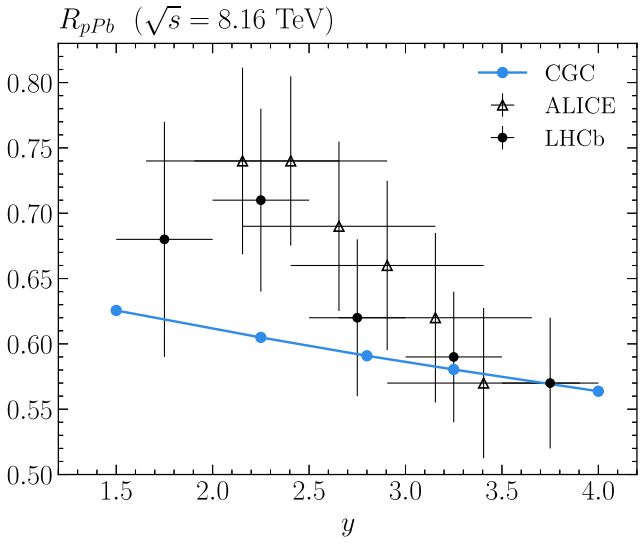

FIG. 7. Nuclear supression factor R_{pPb} as a function of rapidity y integrated over the momentum range $0 < p_\perp < 10$ GeV at $\sqrt{s} = 8.16$ TeV. The vertical error bars are quadratic sums of statistical and systematic uncertainties in both LHCb data [5] for prompt J/ψ production and ALICE data [9] for inclusive J/ψ production. The horizontal error bars are bin widths.

although the $p_\perp$ dependence in our calculation is slightly steeper. The reason for this could be the missing next-to-leading order effects, which are expected to lead to a weaker $p_\perp$ dependence due to the additional phase space available for the emission of an extra parton [34,64].

In Fig. 7, we illustrate the rapidity dependence of the $p_\perp$-integrated R_{pPb} predicted by the BK evolution. The rapidity dependence is weaker than in the data similarly as in Ref. [21], where the color evaporation model was applied with the same CGC setup that is used here. The agreement is better at most forward rapidities, where the dilute-dense factorization is expected to be most accurate.

IV. SUMMARY AND DISCUSSION

In this paper, we have calculated the cross section for forward J/ψ production in proton-proton and minimum bias proton-lead collisions in the CGC + NRQCD formalism. The CGC description of the dense proton and nuclear target is constrained by HERA DIS data, and the hadronization process is encoded in the LDMEs. Thus, there are no free parameters in our setup, and we calculate J/ψ production consistently with the DIS data.

We find that the dominant contribution to the cross section is the color octet channel ${}^1S_0^{[8]}$, which contributes roughly 70% to the cross section in $p + p$ and $p +$ pb collisions. Interestingly, the color singlet ${}^3S_1^{[1]}$ contribution is small, with only an approximate 15% contribution to the total. Although this contrasts the hierarchy expected from NRQCD power counting in Eq. (11), we expect that the contribution from the singlet channel should become larger at large $p_\perp$ in a NLO calculation.

At small $p_\perp$, our predictions for the cross sections calculated as a sum of the individual channels shown in Figs. 3 and 4 overestimate the experimental LHCb and ALICE data in both $p + p$ and $p +$ pb collisions. The cross section is also predicted to peak at lower p_T than seen in the data. However, we obtain a good agreement with the data at large p_T already at LO in the CGC theory. This can help to better understand the transition from the CGC theory at small $p_\perp$ to collinear factorization at high $p_\perp$ for this process.

We expect that DIS fits including the heavy quark contribution could improve the normalization of the cross section. Similarly, it could be valuable to revisit the determination of the LDMEs in a consistent fit within the CGC formalism, potentially including polarization observables [51]. Furthermore, moving to NLO can be expected to have a numerically significant effect; for example, the Sudakov factor is expected to push the maximum of the cross section to a larger $p_\perp$.

Unlike absolute cross sections, our predictions for the nuclear modification ratio R_{pPb} as a function of $p_\perp$ shown in Fig. 6 are within the error bands of ALICE and LHCb data for most forward rapidites $y \geq 2.7$. However, we predict a slightly stronger dependence on the J/ψ transverse momentum than seen in the experimental data. The rapidity dependence of R_{pPb} shown in Fig. 7 is in agreement with the experimental data at most forward rapidities $y \gtrsim 3$, but a significantly weaker rapidity dependence is

predicted closer to midrapidity where the applied dilute-dense factorization is less accurate. This reinforces the validity of the dilute-dense description in the CGC in the forward region and demonstrates the possibility to use forward inclusive J/ψ data to probe gluon saturation phenomena at LHC energies.

ACKNOWLEDGMENTS

We thank J. Penttala, F. Salazar and Z. Kang for useful discussions. This work was supported by the Research Council of Finland, the center of Excellence in Quark Matter (Projects No. 346324 and No. 364191), and Projects No. 338263, No. 346567, and No. 359902, and under the European Union's Horizon 2020 research and innovation programme by the European Research Council (ERC, Grant Agreements No. ERC-2023-101123801 GlueSatLight and ERC-2018-ADG-835105 YoctoLHC) and by the STRONG-2020 project (Grant Agreement No. 824093). Computing resources from CSC—IT Center for Science in Espoo, Finland and the Finnish Grid and Cloud Infrastructure (persistent identifier `urn:nbn:fi:research-infras-2016072533`) were used in this work. The content of this article does not reflect the official opinion of the European Union, and responsibility for the information and views expressed therein lies entirely with the authors.

DATA AVAILABILITY

No data were created or analyzed beyond what is included in this article.

[1] J. Adam *et al.* (STAR Collaboration), J/ψ production cross section and its dependence on charged-particle multiplicity in $p+p$ collisions at $\sqrt{s}=200$ GeV, Phys. Lett. B **786**, 87 (2018).

[2] U. Acharya *et al.* (PHENIX Collaboration), Measurement of J/ψ at forward and backward rapidity in $p+p$, $p+\mathrm{Al}$, $p+\mathrm{Au}$, and $^3\mathrm{He}+\mathrm{Au}$ collisions at $\sqrt{s_{NN}}=200$ GeV, Phys. Rev. C **102**, 014902 (2020).

[3] U. A. Acharya *et al.* (PHENIX Collaboration), J/ψ and $\psi(2S)$ production at forward rapidity in $p+p$ collisions at $\sqrt{s}=510$ GeV, Phys. Rev. D **101**, 052006 (2020).

[4] R. Aaij *et al.* (LHCb Collaboration), Measurement of forward J/ψ production cross-sections in pp collisions at $\sqrt{s}=13$ TeV, J. High Energy Phys. 10 (2015) 172; 05 (2017) 63.

[5] R. Aaij *et al.* (LHCb Collaboration), Prompt and non-prompt J/ψ production and nuclear modification in pPb collisions at $\sqrt{s_{\mathrm{NN}}}=8.16$ TeV, Phys. Lett. B **774**, 159 (2017).

[6] B. B. Abelev *et al.* (ALICE Collaboration), J/ψ production and nuclear effects in p-Pb collisions at $\sqrt{S_{NN}}=5.02$ TeV, J. High Energy Phys. 02 (2014) 073.

[7] S. Acharya *et al.* (ALICE Collaboration), Inclusive J/ψ production at midrapidity in pp collisions at $\sqrt{s}=13$ TeV, Eur. Phys. J. C **81**, 1121 (2021).

[8] S. Acharya *et al.* (ALICE Collaboration), J/ψ production at midrapidity in *p-Pb* collisions at $\sqrt{s_{\mathrm{NN}}}=8.16$ TeV, J. High Energy Phys. 07 (2023) 137.

[9] S. Acharya *et al.* (ALICE Collaboration), Inclusive J/ψ production at forward and backward rapidity in p-Pb collisions at $\sqrt{s_{\mathrm{NN}}}=8.16$ TeV, J. High Energy Phys. 07 (2018) 160.

[10] Y. V. Kovchegov and E. Levin, *Quantum Chromodynamics at High Energy* (Oxford University Press, New York, 2013), Vol. 33.

[11] F. Gelis, E. Iancu, J. Jalilian-Marian, and R. Venugopalan, The Color glass condensate, Annu. Rev. Nucl. Part. Sci. **60**, 463 (2010).

[12] H. Weigert, Evolution at small x(bj): The Color glass condensate, Prog. Part. Nucl. Phys. **55**, 461 (2005).

[13] E. Iancu and R. Venugopalan, The Color glass condensate and high-energy scattering in QCD, arXiv:hep-ph/0303204.

[14] J. P. Blaizot, F. Gelis, and R. Venugopalan, High-energy pA collisions in the color glass condensate approach. 2. Quark production, Nucl. Phys. **A743**, 57 (2004).

[15] C.-H. Chang, Hadronic production of J/ψ associated with a gluon, Nucl. Phys. **B172**, 425 (1980).

[16] R. Baier and R. Ruckl, Hadronic production of J/ψ and Υ: Transverse momentum distributions, Phys. Lett. **102B**, 364 (1981).

[17] J.-P. Lansberg, New observables in inclusive production of quarkonia, Phys. Rep. **889**, 1 (2020).

[18] Y.-Q. Ma and R. Vogt, Quarkonium production in an improved Color evaporation model, Phys. Rev. D **94**, 114029 (2016).

[19] V. Cheung and R. Vogt, Production and polarization of prompt J/ψ in the improved color evaporation model using the k_T-factorization approach, Phys. Rev. D **98**, 114029 (2018).

[20] H. Fujii and K. Watanabe, Heavy quark pair production in high energy pA collisions: Quarkonium, Nucl. Phys. **A915**, 1 (2013).

[21] B. Ducloué, T. Lappi, and H. Mäntysaari, Forward J/ψ production in proton-nucleus collisions at high energy, Phys. Rev. D **91**, 114005 (2015).

[22] G. T. Bodwin, E. Braaten, and G. P. Lepage, Rigorous QCD analysis of inclusive annihilation and production of heavy quarkonium, Phys. Rev. D **51**, 1125 (1995); **55**, 5853(E) (1997).

[23] M. Krämer, Quarkonium production at high-energy colliders, Prog. Part. Nucl. Phys. **47**, 141 (2001).

[24] N. Brambilla *et al.*, Heavy quarkonium: Progress, puzzles, and opportunities, Eur. Phys. J. C **71**, 1534 (2011).

[25] Z.-B. Kang, Y.-Q. Ma, and R. Venugopalan, Quarkonium production in high energy proton-nucleus collisions: CGC meets NRQCD, J. High Energy Phys. 01 (2014) 056.

[26] Y.-Q. Ma and R. Venugopalan, Comprehensive description of J/ψ production in proton-proton collisions at collider energies, Phys. Rev. Lett. **113**, 192301 (2014).
[27] Y.-Q. Ma, R. Venugopalan, and H.-F. Zhang, J/ψ production and suppression in high energy proton-nucleus collisions, Phys. Rev. D **92**, 071901 (2015).
[28] F. Dominguez, C. Marquet, B.-W. Xiao, and F. Yuan, Universality of unintegrated gluon distributions at small x, Phys. Rev. D **83**, 105005 (2011).
[29] I. Balitsky, Operator expansion for high-energy scattering, Nucl. Phys. **B463**, 99 (1996).
[30] Y. V. Kovchegov, Small-x F_2 structure function of a nucleus including multiple pomeron exchanges, Phys. Rev. D **60**, 034008 (1999).
[31] T. Lappi and H. Mäntysaari, Single inclusive particle production at high energy from HERA data to proton-nucleus collisions, Phys. Rev. D **88**, 114020 (2013).
[32] H. Mäntysaari and H. Paukkunen, Saturation and forward jets in proton-lead collisions at the LHC, Phys. Rev. D **100**, 114029 (2019).
[33] B. Ducloué, T. Lappi, and H. Mäntysaari, Forward J/ψ production at high energy: Centrality dependence and mean transverse momentum, Phys. Rev. D **94**, 074031 (2016).
[34] H. Mäntysaari and Y. Tawabutr, Complete next-to-leading order calculation of single inclusive $\pi 0$ production in forward proton-nucleus collisions, Phys. Rev. D **109**, 034018 (2024).
[35] S. Bailey, T. Cridge, L. A. Harland-Lang, A. D. Martin, and R. S. Thorne, Parton distributions from LHC, HERA, Tevatron and fixed target data: MSHT20 PDFs, Eur. Phys. J. C **81**, 341 (2021).
[36] I. Balitsky, Quark contribution to the small-x evolution of color dipole, Phys. Rev. D **75**, 014001 (2007).
[37] L. D. McLerran and R. Venugopalan, Computing quark and gluon distribution functions for very large nuclei, Phys. Rev. D **49**, 2233 (1994).
[38] F. D. Aaron *et al.* (H1 and ZEUS Collaborations), Combined measurement and QCD analysis of the inclusive $e^{\pm}p$ scattering cross sections at HERA, J. High Energy Phys. 01 (2010) 109.
[39] A. Dumitru and J. Jalilian-Marian, Forward dijets in high-energy collisions: Evolution of QCD n-point functions beyond the dipole approximation, Phys. Rev. D **82**, 074023 (2010).
[40] C. Marquet and H. Weigert, New observables to test the Color Glass Condensate beyond the large- N_c limit, Nucl. Phys. **A843**, 68 (2010).
[41] H. Fujii, F. Gelis, and R. Venugopalan, Quark pair production in high energy pA collisions: General features, Nucl. Phys. **A780**, 146 (2006).
[42] A. H. Mueller, A simple derivation of the JIMWLK equation, Phys. Lett. B **523**, 243 (2001).
[43] A. Dumitru, J. Jalilian-Marian, T. Lappi, B. Schenke, and R. Venugopalan, Renormalization group evolution of multi-gluon correlators in high energy QCD, Phys. Lett. B **706**, 219 (2011).
[44] T. Lappi and H. Mantysaari, Forward dihadron correlations in deuteron-gold collisions with the Gaussian approximation of JIMWLK, Nucl. Phys. **A908**, 51 (2013).
[45] P. L. Cho and A. K. Leibovich, Color octet quarkonia production, Phys. Rev. D **53**, 150 (1996).
[46] E. J. Eichten and C. Quigg, Quarkonium wave functions at the origin, Phys. Rev. D **52**, 1726 (1995).
[47] K.-T. Chao, Y.-Q. Ma, H.-S. Shao, K. Wang, and Y.-J. Zhang, J/ψ polarization at hadron colliders in nonrelativistic QCD, Phys. Rev. Lett. **108**, 242004 (2012).
[48] Y. V. Kovchegov, J. Kuokkanen, K. Rummukainen, and H. Weigert, Subleading-N_c corrections in non-linear small-x evolution, Nucl. Phys. **A823**, 47 (2009).
[49] T. Lappi, H. Mäntysaari, and A. Ramnath, Next-to-leading order Balitsky-Kovchegov equation beyond large N_c, Phys. Rev. D **102**, 074027 (2020).
[50] T. Stebel and K. Watanabe, J/ψ polarization in high multiplicity pp and pA collisions: CGC + NRQCD approach, Phys. Rev. D **104**, 034004 (2021).
[51] Y.-Q. Ma, T. Stebel, and R. Venugopalan, J/ψ polarization in the CGC + NRQCD approach, J. High Energy Phys. 12 (2018) 057.
[52] Y.-Q. Ma, K. Wang, and K.-T. Chao, A complete NLO calculation of the J/ψ and ψ' production at hadron colliders, Phys. Rev. D **84**, 114001 (2011).
[53] M. A. Nefedov, V. A. Saleev, and A. V. Shipilova, Charmonium production at the Tevatron and Large Hadron Collider in the Regge limit of QCD, Phys. At. Nucl. **76**, 1546 (2013).
[54] J. P. Lansberg, On the mechanisms of heavy-quarkonium hadroproduction, Eur. Phys. J. C **61**, 693 (2009).
[55] K. Watanabe and B.-W. Xiao, Forward heavy quarkonium productions at the LHC, Phys. Rev. D **92**, 111502 (2015).
[56] P. Sun, C. P. Yuan, and F. Yuan, Heavy quarkonium production at low Pt in NRQCD with soft gluon resummation, Phys. Rev. D **88**, 054008 (2013).
[57] B. Gong, L.-P. Wan, J.-X. Wang, and H.-F. Zhang, Polarization for prompt J/ψ and $\psi(2s)$ production at the tevatron and LHC, Phys. Rev. Lett. **110**, 042002 (2013).
[58] G. T. Bodwin, K.-T. Chao, H. S. Chung, U.-R. Kim, J. Lee, and Y.-Q. Ma, Fragmentation contributions to hadroproduction of promptJ/ψ, χ_{cJ}, and $\psi(2S)$ states, Phys. Rev. D **93**, 034041 (2016).
[59] M. Butenschoen and B. A. Kniehl, Probing nonrelativistic QCD factorization in polarized J/ψ photoproduction at next-to-leading order, Phys. Rev. Lett. **107**, 232001 (2011).
[60] C. Casuga, M. Karhunen, and H. Mäntysaari, Inferring the initial condition for the Balitsky-Kovchegov equation, Phys. Rev. D **109**, 054018 (2024).
[61] H. Hänninen, H. Mäntysaari, R. Paatelainen, and J. Penttala, Proton structure functions at next-to-leading order in the dipole picture with massive quarks, Phys. Rev. Lett. **130**, 192301 (2023).
[62] A. H. Mueller, B.-W. Xiao, and F. Yuan, Sudakov resummation in small-x saturation formalism, Phys. Rev. Lett. **110**, 082301 (2013).
[63] J. L. Albacete, N. Armesto, A. Kovner, C. A. Salgado, and U. A. Wiedemann, Energy dependence of the Cronin effect from nonlinear QCD evolution, Phys. Rev. Lett. **92**, 082001 (2004).
[64] B. Ducloué, T. Lappi, and H. Mäntysaari, Isolated photon production in proton-nucleus collisions at forward rapidity, Phys. Rev. D **97**, 054023 (2018).